Investigation of oil-water flow in concentric and fully eccentric annuli pipes

Roberto Ibarra, Jan Nossen *

Institute for Energy Technology (IFE), Kjeller 2007, Norway

ARTICLE INFO

ABSTRACT

Experimental investigations are performed on co-current flow of oil (Exxsol D60) and water in concentric and fully eccentric annuli with the inner pipe located at bottom of the outer pipe. The annulus outer and inner pipe have an inside diameter of 99 mm and outside diameter of 50 mm, respectively. This yields a diameter ratio of $K = 0.505$. The flow conditions studied span mixture velocities and input water cuts in the range 0.50–1.75 m/s and 10–90%, respectively, at pipe inclinations of 0° and 4° upward. Flow regimes have been identified and maps constructed using instantaneous images of the flow from high-speed cameras (shadowgraph) and X-ray chordal holdup measurements along the vertical projection. Flow regimes in the concentric annulus exhibit a higher level of mixing than that observed in the fully eccentric configuration. The transition to dispersed flow occurs at lower mixture velocities in the concentric annulus. Measurements from broad-beam gamma densitometers reveal that the mean water holdup is higher in the fully eccentric annulus for a given mixture velocity and input water cut. The higher water accumulation in this annulus configuration can be attributed to a low velocity region in the narrow gap at the annulus pipe bottom. The frictional pressure gradient in the concentric annulus is higher as compared with the fully eccentric configuration. Peaks in the pressure gradient profile, for a constant mixture velocity, are observed at high water cuts (*i.e.* WC $\geq$ 50%) at the transition between dual continuous and dispersed flows. Pressure gradient data are compared with predictions using the homogeneous and two-fluid model. In general, the homogeneous model using a modified Brinkman (Brinkman, 1952)/Roscoe (Roscoe, 1952) dispersion viscosity model shows the best agreement with data in both concentric and fully eccentric annuli.

1. Introduction

The co-current flow of two immiscible liquids in pipes is commonly encountered in a number of industrial applications, *e.g.* reactors, mixers, and crude oil wells and pipelines. Liquid-liquid flows are characterised by complex interactions between both liquids in which interfacial forces and wetting characteristics play an important role in the development of the flow. The density ratio in liquid-liquid flows is close to unity, in contrast to gas-liquid flows. Large density difference promotes separation, and thus there is a strong tendency to form stratified flow where the lighter phase flows above and significantly faster than the heavier phase. In liquid-liquid flows, both phases flow at similar velocities for which complex phases configurations are observed.

Liquid-liquid flows have been studied by several researchers, see, for example, Russell et al. (1959), Charles et al. (1961), Arirachakaran et al. (1989), Trallero (1995), Angeli and Hewitt (2000), Lovick and Angeli (2004), Lum et al. (2006), and Kumara et al. (2009). These studies have characterised the flow in terms of the distribution of the phases in the pipe or flow regimes, phase fraction, and pressure gradient for a wide range of flow conditions, fluids properties, and pipe characteristics. Advanced measurement techniques (laser-based) have also been employed to extract detailed space-and time-resolved phase and velocity information on both liquid phases, *e.g.* Liu et al. (2006), Kumara et al. (2010), Pouplin et al. (2011), Morgan et al. (2013), Morgan et al. (2017), and Ibarra et al. (2018). Yet, the behaviour of liquid-liquid flows in pipes is still not fully understood.

Prediction models for flow regime transitions (*e.g.* Trallero, 1995; Torres et al., 2016), phase fraction, and pressure gradient for liquid-liquid flows in circular pipes have been developed and

* Corresponding author at: Department of Fluid Flow and Environmental Technology, Institute for Energy Technology, Instituttveien 18, Kjeller 2007, Norway.

E-mail addresses: roberto.jose.ibarra-hernandez@ife.no (R. Ibarra), jan.nossen@ife.no (J. Nossen).

validated using large experimental data sets (see Izwan Ismail et al., 2015; and Prieto et al., 2018; for a review of liquid-liquid flow phase fraction and pressure gradient correlations). However, very limited data are available for liquid-liquid flows in annulus configurations. An annulus pipe consists of two parallel pipes where the fluids flow through the region between the inside wall of the outer pipe and the outside wall of the inner pipe. Flow in annulus configurations can be encountered in heat exchangers, reactors, and oil wells. The latter is of special interest as, for example, mixtures of oil and water (and/or drilling fluids) may flow in the annular space between the production tubing and the outer casing in some cases.

Multiphase flow in annulus configurations differs from that in circular pipes. The presence of the inner pipe affects the pressure gradient in the pipe system, even for single-phase flows, *i.e.* a concentric annulus configuration yields a larger pressure gradient than in a circular pipe with equivalent hydraulic diameter at similar Reynolds number. The opposite behaviour is observed for fully eccentric annulus, *i.e.* the pressure gradient is lower than in an equivalent circular pipe (Caetano et al., 1992a, 1992b). Ibarra et al. (2019) found that the wetting characteristics of the pipe might also have an influence on the structure of the phases for gas-liquid flows in annuli. Gas-water flow in concentric annulus showed chaotic or unstable behaviour in regions dominated by well-defined slug structures in gas-oil flow. It was observed that the oil wetted the pipe creating a continuous thin film at the pipe wall in the gas region. For gas-water flows, this thin film was not continuous. This effect is more prominent in concentric annulus. Moreover, it was observed that the structure of the flow in eccentric annulus was more stable than that in the concentric annulus configuration for a given fluids combination.

The study of multiphase flow in annulus has been focused on gas–liquid flows, principally for vertical configurations (see, for example, Kelessidis and Dukler, 1989; Caetano et al., 1992a, b; Hasan and Kabir, 1992; Hibiki et al., 2003; Julia et al., 2011). In liquid-liquid flows, the effect of an inner pipe and its eccentricity on the behaviour of the flow has not been thoroughly studied. Shahidi and Ozbelge (1995) studied the heat transfer between water and a heat transfer oil through a horizontal concentric annulus of high aspect ratio. Moyers-Gonzalez and Frigaard (2007) studied kinematic instabilities in primary-cementing displacements flows in inclined oil wells. They found that with increasing annulus eccentricity, stable flows became more stable and unstable flows became more unstable.

There is clearly a lack of experimental data in terms of flow regimes, phase fraction, and pressure gradient in liquid-liquid flows in annuli. These data are required to develop and/or validate prediction models of the flow parameters. Thus, understanding these types of flows can lead to safer and more efficient operations.

The rest of this paper is structured as follows. Section 2 describes the experimental flow facility, instrumentation, and procedure. The experimental results and analysis of the flow characteristics are presented in Section 3. Finally, Section 4 presents the main conclusions of this study.

2. Experimental setup

2.1. Flow facility and test fluids

The co-current oil-water experimental investigations were performed in the Well Flow Loop, located at IFE, which can also be used for gas-liquid and three-phase flow experiments. The test fluids used in this investigation were tap water and oil (Exxsol D60). Their physical properties are shown in Table 1.

Table 1
Physical properties of the test fluids at $\sim 20\,°C$.

	Density, ρ (kg/m³) at ~ 400 kPa (abs.)	Viscosity, μ (mPa.s) at Atm	Interfacial tension, σ (mN/m) at Atm
Exxsol D60	802 ± 2.4	1.40 ± 0.02	46.1 ± 0.3
Water	998 ± 2.0	1.04 ± 0.02	

The flow loop consists of a liquid-liquid horizontal gravity-driven separator with a capacity of 4 m³ which also acts as a storage tank. For the test fluids and flow rates used in this investigation, retention times for the fluids in the liquid-liquid separator are high enough to guarantee efficient separation. In addition, Coriolis meters installed in the oil line constantly measure the oil density. During our experiments, even at the highest mixture velocity tested, no density changes were observed in the input line. After separation, both liquids are injected into the test section using two centrifugal pumps (one for each liquid) with a capacity of 45 m³/h each. The water volumetric flow rate is measured with an electromagnetic flowmeter with a capacity of 0–60 m³/h, and an accuracy of ±0.5% of the reading. The oil mass flow rate is measured with a set of two Coriolis meters with capacities of 40–20,000 and 80–40,000 kg/h (equivalent to 0.05–25 and 0.1–50 m³/h based on the Exxsol D60 density) and accuracy of ±0.2% of the reading. The oil and water injection lines are equipped with heat exchangers to maintain the temperature within ±1 °C throughout the experimental campaign.

The two liquids are introduced into the test section using a specially-designed inlet which consists of three-chambers (with splitter platers) for water (bottom), oil (middle), and gas (top) phases. Note that the top chamber was not used in this investigation. Details of the inlet section can be found in Ibarra et al. (2019). The implementation of splitter plates at the inlet section promotes initially stratified flow. A flow straightener is installed downstream of the inlet section to remove any swirl generated by the inlet geometry configuration. The annulus pipe has an inside diameter of the outer pipe, D_1, of 99 mm and an outside diameter of the inner pipe, D_2, of 50 mm resulting in a diameter ratio of $K = D_2/D_1 = 0.505$. The test section, as shown in Fig. 1, has a total length of 45 m and is made of clear PVC (inner and outer pipe) with an absolute roughness of approximately 2 μm. The inner pipe extends over the entire length of the test section and was supported using specially-designed wings to minimise the effect on the flow. The non-circular geometry of the annulus is defined using the hydraulic diameter, D_h, which is based on the flow area and the wetted perimeter, $D_h = D_1 - D_2$.

2.2. Instrumentation

The test section (see Fig. 1) is equipped with 5 differential pressure transducers installed at $L/D_h = 284, 410, 501, 649,$ and 719, with L the distance from the inlet. These transducers, which have an accuracy of ±6 Pa, measure the pressure drop, ΔP, over lengths of $62D_h, 40D_h, 50D_h, 38D_h,$ and $64D_h$ respectively. Three broadbeam gamma densitometers, installed at $L/D_h = 256, 520,$ and 704, measure the instantaneous cross-sectional average water holdup, H_W, at a sampling frequency of 50 Hz for a total recording time of 100 s (simultaneously recorded with the pressure gradient data). The holdup measurement is based on the attenuation of the gamma rays between the source and the detector. These gamma densitometers are calibrated by measuring the transmitted intensity for single-phase oil and water. The holdup or phase fraction for two-phase flows is calculated using the respective single-phase intensity calibrations based on a logarithmic expression. The typical intensity values for single-phase (calibration), for
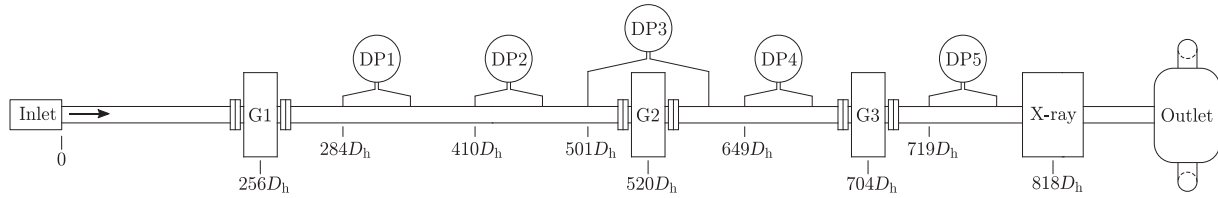
Fig. 1. Schematic of the experimental test section (DP1-5: differential pressure transducers, G1-3: gamma densitometers).

sensor G3, are 130,000 and 119,000 for oil and water, respectively. Note that these values correspond to our experimental setup, *i.e.* single-phase intensity values are affected by the pipe material, wall thickness, and fluids densities, along with the characteristics of the gamma source.

An X-ray system has also been implemented to measure the projected chordal holdup in the annulus cross-section. The X-ray system, which is located at $818D_h$ from the inlet, consists of six X-ray source/detector units installed at different orientation angles around the pipe. However, for this investigation, only the horizontally-oriented unit (which yields a vertical projection), as shown in Fig. 2, is used to assists in the flow regime identification process. The X-ray source emits photons in conical beams which are detected by the opposite detector. The detector has an area of 1510×54 pixels (0.1×0.1 mm per pixel). The X-ray system, set at 60 kV and 4 mA, was operated at a sampling frequency of 50 Hz for a total recording time of 27 s and was triggered with a short delay after the gamma densitometers (approximately 1.5 s).

The X-ray system is calibrated using the same procedure as the gamma densitometers, *i.e.* by measuring the transmitted intensity for single-phase oil and water. However, the X-ray system measures the radiation intensity for each pixel. This allows the calculation of the chordal holdup, α, which is defined as the average volume fraction along the chord between the X-ray source and the detector. For two-phase oil-water flow, the water and oil chordal holdups are given by:

$$\alpha_W = \frac{\log(I_M/I_O)}{\log(I_W/I_O)}, \tag{1}$$

$$\alpha_O = 1 - \alpha_W, \tag{2}$$

where I_M is the measured intensity (at a given pixel), and I_O and I_W are calibration values for the oil and water phase, respectively, for the same pixel. The intensity at the detector sensor is averaged over the narrow camera dimension along the axial length (*i.e.* over 54 pixels) to increase the signal-to-noise level.

Instantaneous images of the flow were captured using four Photron Mini UX100 high-speed cameras. These cameras were installed at L/D_h = 124, 540, 740, and 766 (cameras 1 to 4) and each has a resolution of 1280×1024 pixels at a maximum frame-rate of 4 kHz. The first three cameras were equipped with a 14-mm ultra-wide-angle lens and operated at a frame-rate of 50 Hz to capture large-scale features. The fourth camera, equipped with a Nikkor

60-mm lens, was operated at a frame-rate of 1 kHz to capture fast, small-scale features.

2.3. Flow conditions and experimental procedure

Experimental data have been acquired for various water cuts and mixture velocities at pipe inclinations, θ, of 0° and 4° upward. The water cut is defined as the ratio between the water and total volumetric flow rate at the inlet section, WC = Q_W/Q_T where Q_T = $Q_W + Q_O$, and the mixture velocity as the total volumetric flow rate over the flow area, $U_M = Q_T/A_P$ where A_P the cross-sectional area of the annulus, $A_P = \pi(D_1^2 - D_2^2)/4$.

Experiments cover concentric and fully eccentric annuli with the inner pipe at the bottom of the outer pipe. The annulus eccentricity is defined as the relative position of the inner pipe with respect to the outer pipe, $E = 2\delta/(D_1-D_2)$, where δ is the distance between pipe centres. Thus, for concentric annulus $E = 0$ and for fully eccentric annulus $E = \pm1$. Experiments were performed at steady-state conditions (*i.e.* the water cut and mixture velocity were kept constant during each experimental run) at a pressure of 400 kPa (absolute) and temperature of 21 ± 1 °C measured upstream of the inlet section. The experimental procedure consisted of water cut sweeps, at a constant mixture velocity, decreasing the mixture water cut from an initial value of WC = 100%. Mixture velocities, U_M, were varied between 0.5 and 1.75 m/s and water cuts between 10 and 90% (see Table 2) with increments of 10% with additional WC = 45% and 55% in eccentric annulus at U_M = 1.75 m/s. Note that the water cut range in the eccentric anulus was slightly expanded from that used in the concentric annulus experiments with the purpose of verifying structures at low and high water cuts. However, results reveal no significant difference as will be presented in Section 3.

Uncertainty analysis of the measured flow parameters has been performed based on the systematic errors and standard deviation of the samples which propagate to the calculated quantities (Dieck, 2006). Table 3 shows the average uncertainty estimates of the test pipe characteristics and flow parameters.

3. Results and discussion

3.1. Flow regime classification

The analysis of two-phase flows begins with the identification of the flow regimes. These, defined as the geometrical distribution
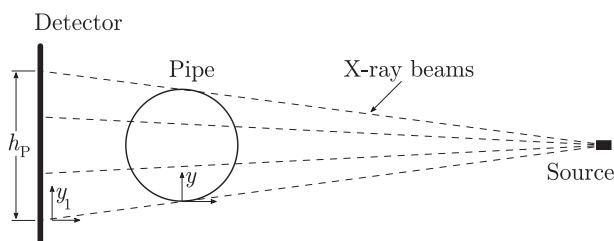

Fig. 2. Schematic of the X-ray side-view system.

Table 2
Experimental mixture velocities and water cuts for each annulus configuration.

U_M (m/s)	WC (%)	
	Concentric	Eccentric
0.50	30–70	20–80
0.75	20–80	20–80
1.00	20–80	10–90
1.25	20–80	10–90
1.50	10–90	10–90
1.75	10–90	10–90

Table 3
Uncertainty estimates.

Variables	Uncertainty
D_1 (mm)	±0.55 mm
D_2 (mm)	±0.28 mm
θ (°)	±0.04°
U_M (m/s)	±1.6%
WC	±1.5%
H_W	±1.9%
$\Delta P/\Delta L$ (Pa/m)	±4.5%

of the phases in the pipe, are affected by the flow velocity, the fluid properties, and the pipe characteristics (*i.e.* the pipe diameter ratio and eccentricity for flow in annuli). In liquid-liquid flows, a number of complex configurations are encountered in contrast to the well-defined structures observed in gas-liquid flows. This is the result of a density ratio closer to unity.

The identification of flow regimes is commonly performed by visual observations. Visualisation techniques, such as shadowgraph and planar laser-induced fluorescence (PLIF), can be used to assist with the identification of the flow regime. These techniques allow the identification of detailed structures which might result in a large number of definitions complicating the flow regime classification. Moreover, the subjective interpretation among different researchers introduces a level of ambiguity leading to unnecessary classifications. Ibarra et al. (2014) proposed a unified flow regime classification for the purpose of simplifying the flow regime classification and enabling direct comparison of flow regime maps.

Fig. 3 shows examples of the flow regimes observed in this study (using shadowgraph) for the entire range of flow velocities in both concentric and fully eccentric annuli following the simple unified classification proposed by Ibarra et al. (2014). Fig. 3(a) presents the stratified-wavy with droplets at/near the interface (SWD). In this flow regime, the flow velocity is such that the generated droplets only flow at or near the interface. As the flow velocity increases, droplets of one phase are dispersed into the other with different levels of entrainment depending on the flow velocity. In this flow regime, both liquids are the continuous phase for a defined pipe cross-sectional region. This regime is called dual continuous flows (DC) (see Fig. 3(b)). Note that dual continuous flows have been categorised as three-layer flows by a number of researchers (*e.g.* Soleimani, 1999; Angeli and Hewitt, 2000; Morgan et al., 2013). In general, for a given flow condition, there is more mixing near the interfacial region for the concentric annulus configuration. This can probably be attributed to the reduced flow cross-sectional area (narrow gap). In Fig. 3(c), droplets of oil are encountered in the upper region of the pipe with a pure water layer below. This flow regime, which has only one continuous phase, is defined as a dispersion of oil-in-water with a water layer (DO/W&W). Finally, Fig. 3(d) shows the dispersed flow regime where droplets flow in the entire cross-section of the annulus pipe. However, droplets can exhibit a heterogeneous distribution depending on the flow velocity and the density ratio, *e.g.* for dispersion of water-in-oil, there could be a higher concentration of droplets at the bottom region of the pipe.

Based on the visualisation technique used in this work for the flow regime classification, it is not possible to identify the type of dispersion in fully-dispersed flows. Shadowgraph is based on the difference of the refractive indices of transparent fluids. The light is refracted as it passes through the fluids interface creating a shadow at the position of the un-refracted light beam. This means that there is no information on which fluid is the continuous and/or the dispersed phase as is the case of PLIF where the addition of a fluorescent dye offers a distinction between the phases (Liu et al.,

2006; Morgan et al., 2013). This is of special interest at high mixture velocities where full dispersions are observed, as will be discussed in Section 3.2.

In fully eccentric annulus, an additional flow regime was observed, *i.e.* dispersion of water-in-oil with a thin water film at the bottom (DW/O&W) as shown in Fig. 4. In this flow regime, both phases are the continuous phase as in dual continuous flows; however, the water film at the bottom region seems to have no oil droplets. This thin water film flows in the narrow gap at the bottom of the pipe, thus, it is slower than the above water-in-oil dispersion layer. This difference in velocity, along with wetting properties, prevents this thin water film from breaking and becoming dispersed in the continuous oil layer.

3.2. Flow regime maps

Flow regimes have been classified for different flow conditions based on visual observations from high-speed images using camera-3 and 4. However, the level of dispersion in the flow, especially at high velocities, might complicate the flow regime identification. Thus, an X-ray system has been used to assist in the flow regime identification process. This complementary approach provides an objective criterion based on the projected chordal holdup in the annulus cross-section (details are described in Section 2.2). A similar X-ray system was employed by Hu et al. (2014) to study the flow structures and phase distributions in two- and three-phase stratified and slug flows. This work was performed in the same flow loop as the present study. In annulus flows, Harvel et al. (1999) used X-ray computed tomography to quantify the void fraction distribution in a vertical concentric annulus with stagnant liquid.

Fig. 5 shows the mean (time-averaged) chordal water holdup, α_W, along the vertical projection in the X-ray detector for the flow conditions displayed in Figs. 3 and 4. For stratified-wavy with droplets, the mean chordal water holdup profile is characterised by an abrupt change with $\alpha_W \approx 0$ and $\alpha_W \approx 1$ at the top and bottom region of the pipe, respectively, as shown in Fig. 5(a). Note that this change is located at different vertical positions for the same inlet flow conditions, *i.e.* the water layer height is higher in the fully eccentric annulus as the inner pipe is located at the bottom region of the outer pipe. Dual continuous flows show a more gradual change along the interfacial region (see Fig. 5(b)). The gradient of the chordal water holdup profile is higher for the fully eccentric annulus case. This indicates that the mixing layer, for the same inlet conditions, is thicker in the concentric annulus. This also suggests that the concentric configuration generates more droplets, *i.e.* stronger interfacial instabilities.

For dispersions of oil-in-water with a water layer (see Fig. 5(c)), the chordal water holdup profile is similar to that observed in separated flows; however, profiles indicate the presence of water in the top region of the pipe (*i.e.* $\alpha_W > 0$). In general, this indicates that water is the continuous phase in the entire cross-section of the annulus and that the concentration of oil increases towards the top of the pipe. The chordal holdup profile for fully dispersed flows, as presented in Fig. 5(d), shows that both oil and water phases are present at every chord along the vertical direction, *i.e.* $0.4 < \alpha_W < 0.9$. These profiles provide an indication of the phase distribution along the vertical axis; however, it is not possible to determine the continuous and dispersed phase. Finally, dispersion of water-in-oil with a water film, which was only observed in the fully eccentric annulus, shows that the chordal water holdup gradually increases towards the bottom of the pipe with $\alpha_W \approx 1$ at the pipe bottom (see Fig. 5(e)).

Flow regime maps have been constructed based on the identification criteria discussed above. Fig. 6 shows the flow regime maps for both concentric and fully eccentric annuli at pipe inclinations, θ,

(a) Stratified-wavy with droplets (SWD)

(b) Dual continuous (DC)

(c) Dispersion of oil-in-water with a water layer (DO/W&W)
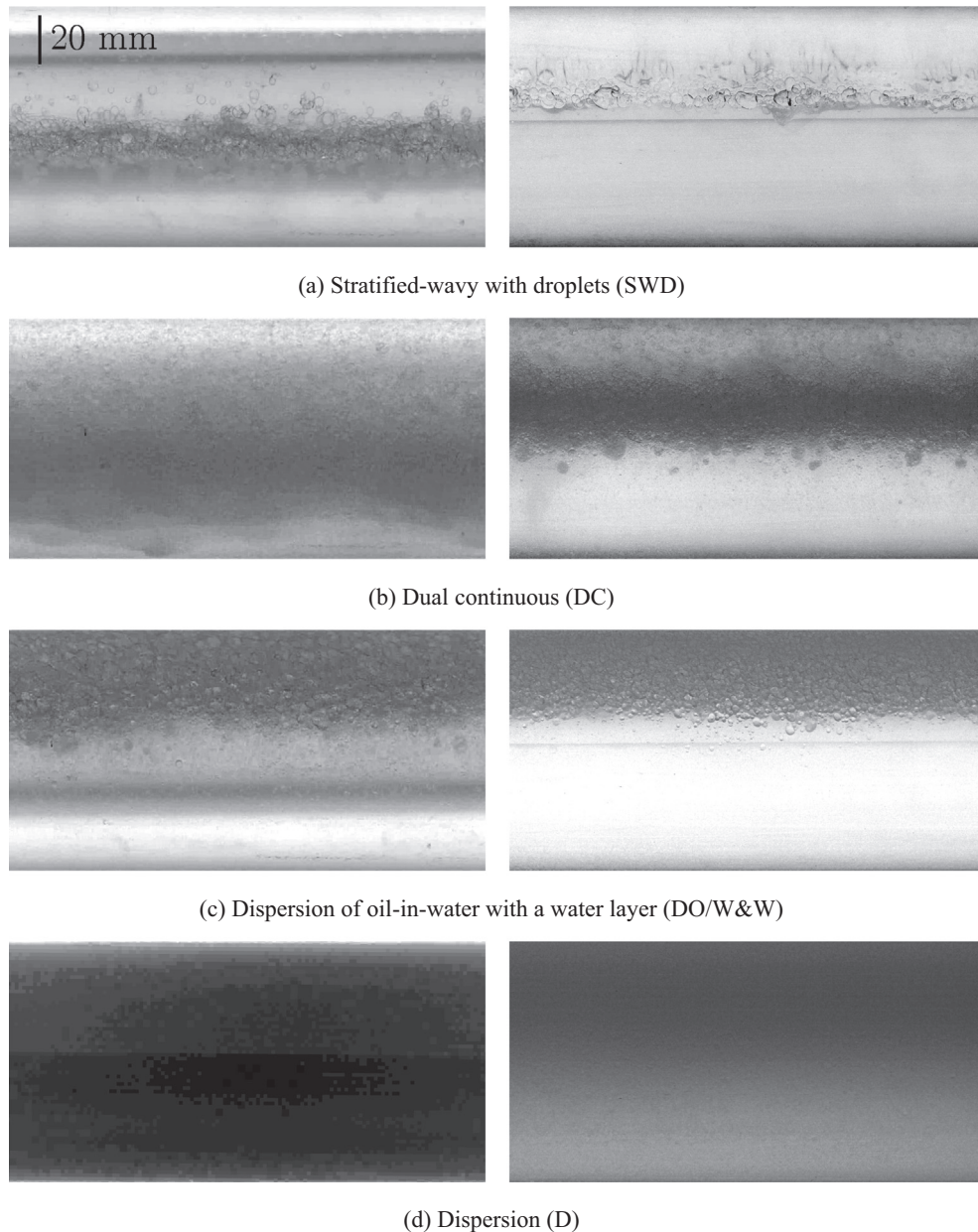

(d) Dispersion (D)

Fig. 3. Flow regimes observed in the experimental campaign from camera-4. Instantaneous flow images correspond to horizontal concentric annulus (left panel) and fully eccentric annulus (right panel) at: (a) U_M = 0.5 m/s, WC = 40%; (b) U_M = 1.0 m/s, WC = 40%; (c) U_M = 0.75 m/s, WC = 80%; and (d) U_M = 1.5 m/s, WC = 70%.
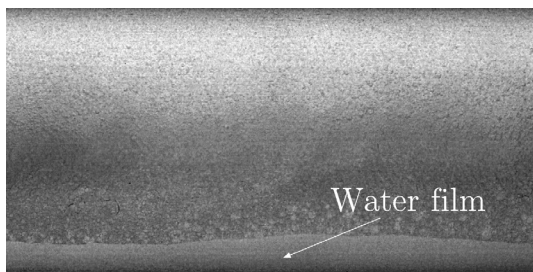

Fig. 4. Dispersion of water-in-oil with a thin water film at the bottom (DW/O&W). Instantaneous flow image corresponds to horizontal fully eccentric annulus at U_M = 1.0 m/s and WC = 10%.

of 0° and 4°. Stratified-wavy with droplets (SWD) is only observed, for all configurations, at the lowest mixture velocity studied, i.e. U_M = 0.5 m/s. With increasing mixture velocity, more droplets are formed, thus a transition to dual continuous flows occurs. The water cut region at which dual continuous flow is observed, for a given mixture velocity, becomes smaller as the mixture velocity increases, i.e. it has a triangular shape. Dispersions of oil-in-water with a water layer (DO/W&W) are only observed at high water cuts (i.e. WC $\geq$ 60%) with a transition to dispersed flows as the mixture velocity increases. Fully dispersed flows (D) are dominant at high mixture velocities, especially in the concentric annulus. This suggests that concentric annulus promotes larger instabilities, as compared to fully eccentric, that prevent both phases from being the continuous phase (dual continuous). This can be attributed to the difference in the velocity distribution which in turn is affected by the annulus cross-sectional area distribution, i.e. wider gap for fully eccentric annulus. Moreover, the pipe wettability might also have an influence in the behaviour of the flow. In the concentric annulus, the oil-water interface is usually located within the range of heights where the inner pipe is located. Conversely, for fully eccen-
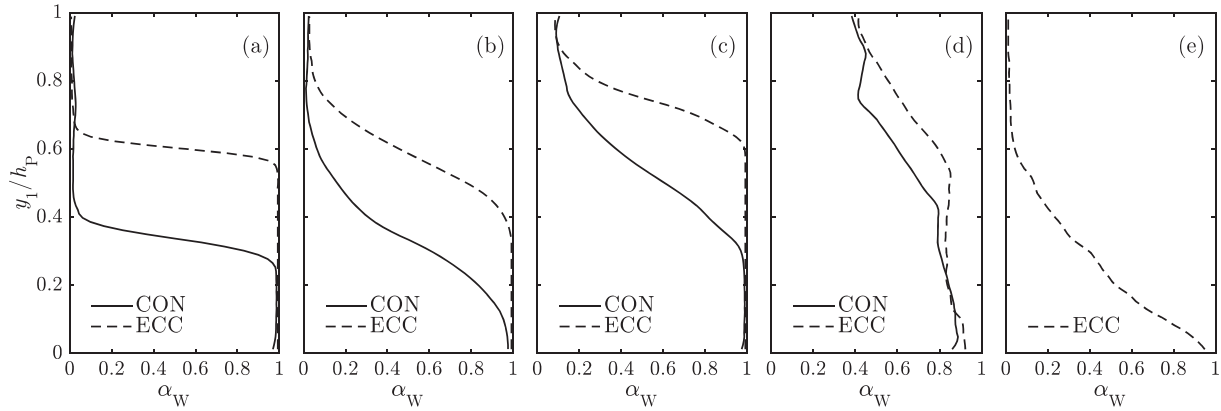
Fig. 5. Typical chordal water holdup, α_W, for the flow conditions shown in Fig. 3 and 4 in concentric and fully eccentric annuli: (a) stratified-wavy with droplets (SWD), (b) dual continuous (DC), (c) Dispersion of oil-in-water with a water layer (DO/W&W), (d) dispersion (D), and (e) dispersion of water-in-oil with a water film (DW/O&W). The y-axis corresponds to the vertical distance from the bottom of the pipe projection in the X-ray detector, y_1, normalised by the projection height, h_P, as shown in Fig. 2.
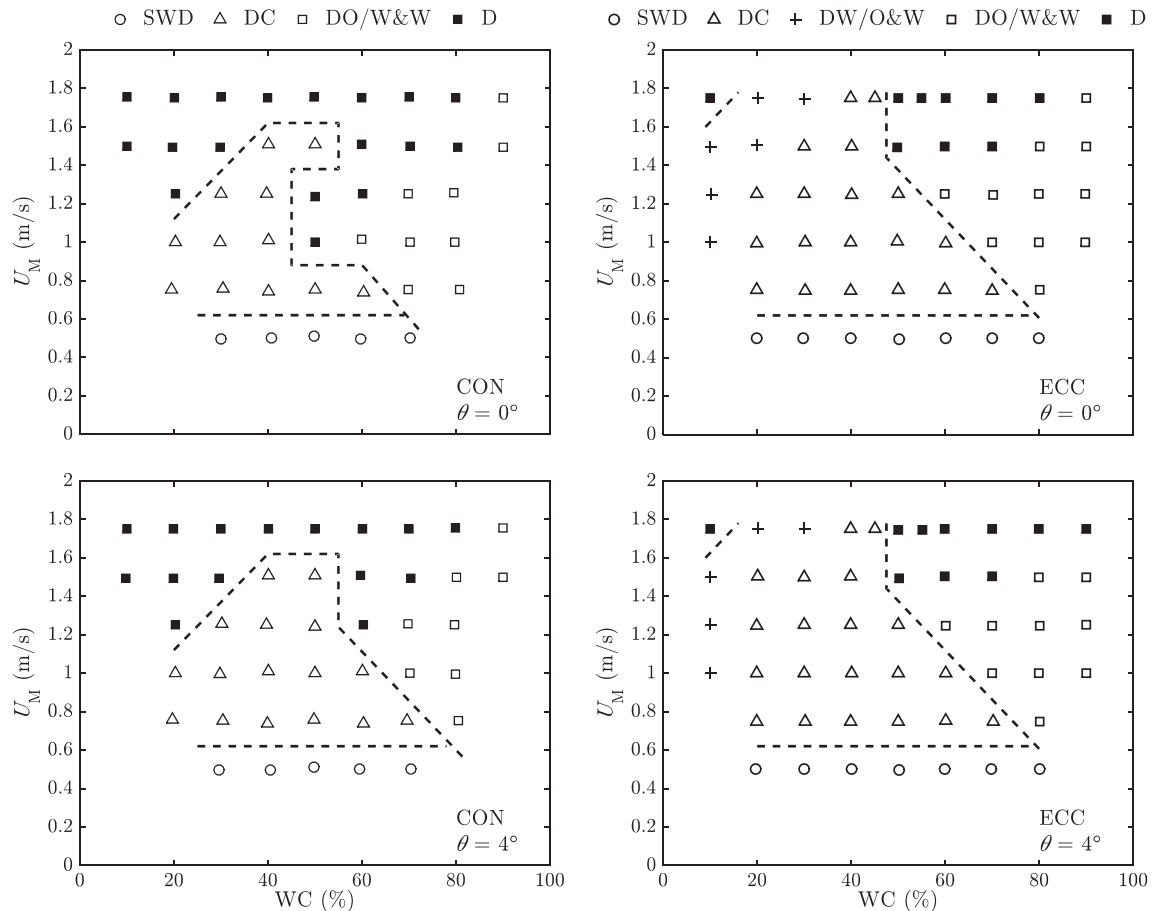

Fig. 6. Flow regime maps in concentric (CON) and fully eccentric (ECC) annuli, shown in the left and right column of panels, respectively, at $\theta = 0°$ (top row) and $\theta = 4°$ (bottom row).

tric annulus, the inner pipe, for most conditions, is covered by the water phase, *i.e.* the interface is located above the inner pipe (see, for example, Fig. 3(a)). Finally, dispersions of water-in-oil with a water film (DW/O&W), which are only observed for fully eccentric annulus, occur at low water cuts (*i.e.* WC ≤ 30%). The overall features of the observed flow regime maps (*i.e.* relative locations of the different flow regimes in terms of water cut and mixture velocity) agree with those from previous studies in circular pipes (*e.g.* Trallero, 1995; Soleimani, 1999).

For a given mixture velocity, the transition between dual continuous and fully dispersed flows represents a partial phase inversion (note that the dashed lines in Fig. 6 only show the transitions to stratified flow and full dispersions). By partial phase inversion we mean the transition from one continuous/one dispersed phase (*i.e.* dispersed flow) to dispersion with two continuous phases (*i.e.* dual continuous flows where the oil and water are the continuous phases at the top and bottom regions of the pipe, respectively). For example, in the fully eccentric configuration, the partial inversion

point at U_M = 1.75 m/s is located at approximately WC = 50%. Conversely, in the concentric annulus at the same mixture velocity (i.e. U_M = 1.75 m/s), the inversion point cannot be identified from the flow regime map. For this, the pressure gradient profile can be used to identify the inversion point as will be discussed in Section 3.4.

3.3. Phase fraction

Fig. 7 shows the mean water holdup, H_W, as function of the water cut in both the concentric and fully eccentric annuli in a horizontal configuration. The holdup data presented here correspond to gamma sensor 3 (G3 from Fig. 1). The mean water holdup in the fully eccentric annulus, for all conditions studied, is higher than those observed in the concentric annulus, especially at low water cuts and low mixture velocities. This can be attributed, as discussed by Ibarra et al. (2019), to a low velocity region in the narrow gap at the pipe bottom in the fully eccentric annulus which in turn increases the water accumulation. This also implies that, for a given flow condition, the oil flows faster in the fully eccentric annulus, i.e. the cross-sectional area occupied by the oil phase decreases as the annulus eccentricity increases. At high mixture velocities (see Fig. 7 at $U_M \geq 1.50$ m/s which corresponds to a transition to dispersed flows) the mean water holdup in the concentric and fully eccentric annuli seems to collapse to a generic trend, i.e. the water holdup is similar in both annulus configurations.

The no-slip line (at which H_W = WC) represents the condition where both fluids flow at the same mean velocity. This is, for example, the case for highly mixed flows where there is minimum slippage between the dispersed and continuous phase. From our data, this behaviour is more apparent in the concentric annulus (at high U_M). Note that the transition to dispersed flow in concentric annulus occurs at lower mixture velocities as compared to fully

eccentric annulus (see Fig. 6). Above the no-slip line (H_W > WC), the oil phase flows faster than the water phase. This is observed for most of the conditions studied in both annulus configurations with the exception of U_M = 0.75, 1.00 and 1.25 m/s at high water cuts in the concentric annulus. At these conditions, which correspond to dispersions of oil-in-water with a water layer (DO/W&W), the water phase flows faster than the oil phase. This behaviour could be attributed to the flow regime. However, the DO/W&W regime is also observed in the fully eccentric annulus, for which H_W > WC. Further inspection of the high-speed images reveals a particular configuration during this flow regime in concentric annulus (see Fig. 8), i.e. a wavy interface between the oil-in-water dispersion layer at the top of the pipe and the water layer below. This wavy interface is especially prominent at U_M = 0.75 m/s (i.e. higher interfacial waves amplitude).

This behaviour indicates that concentric annulus yields an unstable interface for DO/W&W. This can be attributed to wall shear effects at the outer wall of the inner pipe and the presence of secondary flows in the water layer. Conan et al. (2007) studied liquid-liquid dispersed-stratified flow in a horizontal circular pipe. The flow configuration consisted of a continuous layer of an aqueous phase with a highly concentrated layer of oil droplets flowing above (i.e. DO/W&W). They observed, using particle image velocimetry, the presence of secondary flows in the aqueous layer (i.e. two symmetrical pairs of counter-rotating vortices). However, the effect of these secondary flows on the flow stability in annuli flows is unclear. This behaviour requires further investigation.

Fig. 9 shows a comparison of the mean water holdup at different pipe inclinations. At low mixture velocities in inclined pipes, gravitational forces become significant and can dominate over inertial forces. This yields an increase in the water holdup (see Fig. 9 for $U_M \leq 0.75$ m/s) as the velocity of the heavier phase
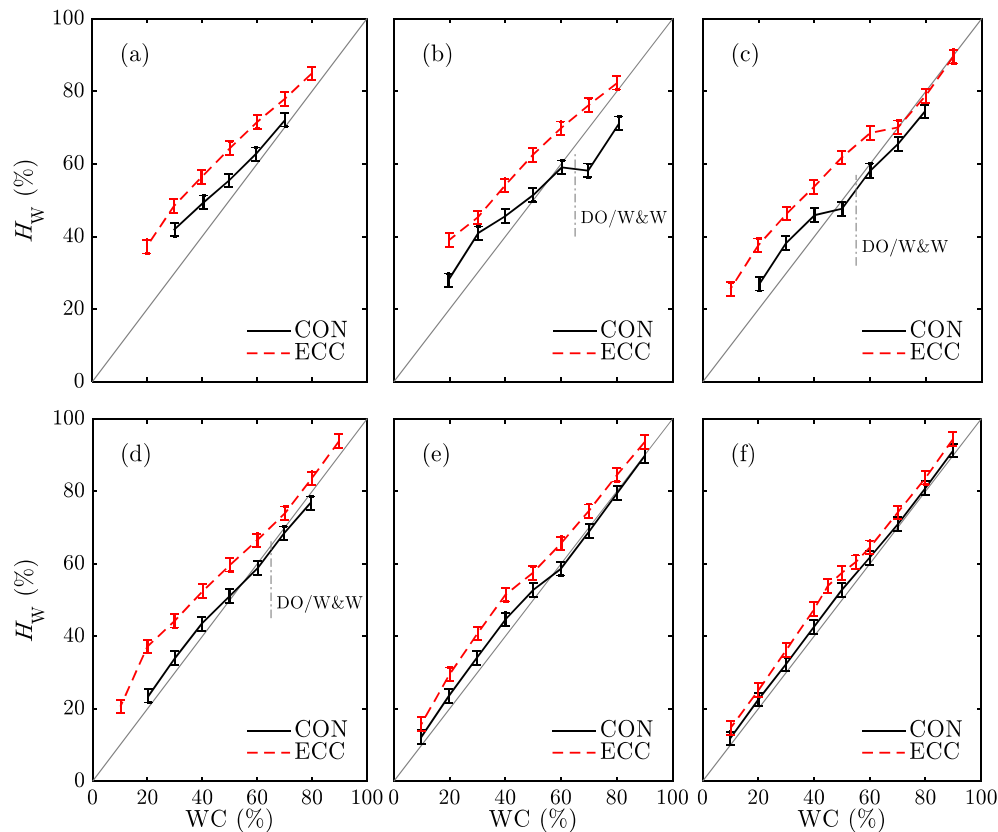

Fig. 7. Mean water holdup, H_W, as function of the input water cut, in horizontal concentric and fully eccentric annuli at mixture velocities, U_M, of: (a) 0.50 m/s, (b) 0.75 m/s, (c) 1.00 m/s, (d) 1.25 m/s, (e) 1.50 m/s, and (f) 1.75 m/s.
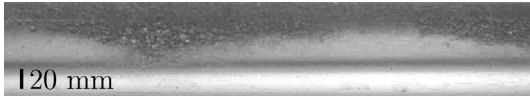
Fig. 8. Instantaneous flow image (from camera-3) in horizontal concentric annulus at U_M = 0.75 m/s and WC = 80%. Flow regime corresponds to DO/W&W with a very wavy interface between the layer of oil-in-water droplets and the water layer.

decreases. As the mixture velocity increases, inertial forces overcome the effect of gravity on the flow, thus, the mean water holdup becomes independent on the pipe inclination (see Fig. 9 at $U_M \geq 1.25$ m/s). This behaviour is more noticeable in the concentric annulus.

A particular behaviour is observed in the fully eccentric annulus configuration. As the mixture velocity increases, the mean water holdup at $\theta = 4°$ is slightly lower than that observed at 0°. This indicates that the water velocity increases, thus, there is a higher level of mixing in the pipe as compared to the horizontal case. This is observed in Fig. 10 for U_M = 1.25 m/s and WC = 20%. For this specific case, a three-layer flow type is observed in the horizontal configuration. Conversely for $\theta = 4°$, the dispersion layer extends from the top to the bottom of the pipe with a thin water layer in the narrow gap.

3.4. Pressure gradient

The mean frictional pressure gradient, $\Delta P/\Delta L$, is presented in Fig. 11 in both the concentric and fully eccentric annuli at $\theta = 0°$ and 4°. The frictional pressure gradient is calculated from the total pressure gradient as
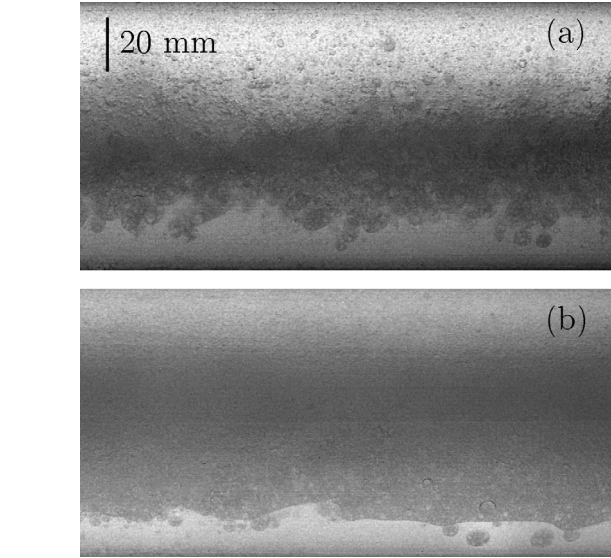

Fig. 10. Instantaneous flow images (from camera-4) in fully eccentric annulus at U_M = 1.25 m/s and WC = 20% at pipe inclinations, θ, of: (a) 0° and (b) 4°.

$$\left[\frac{\Delta P}{\Delta L}\right]_{Fric} = \left[\frac{\Delta P}{\Delta L}\right]_{Total} - \rho_M g \sin\theta, \tag{3}$$

where g is the gravitational acceleration and ρ_M is the mixture density,

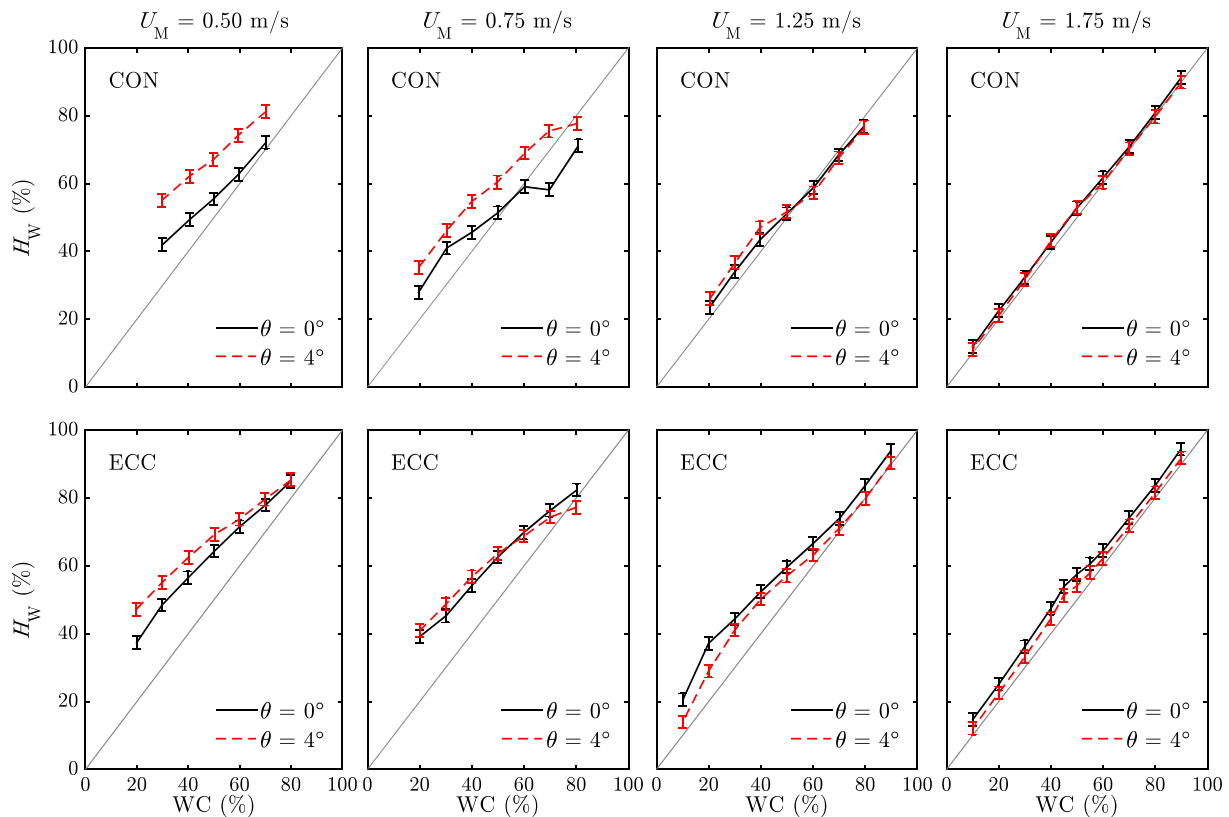$$\rho_M = \rho_W H_W + \rho_O (1 - H_W). \tag{4}$$

Fig. 9. Mean water holdup, H_W, as function of the water cut, in concentric and fully eccentric annuli, shown in the top and bottom rows, respectively, at pipe inclinations, θ, of 0° and 4°.
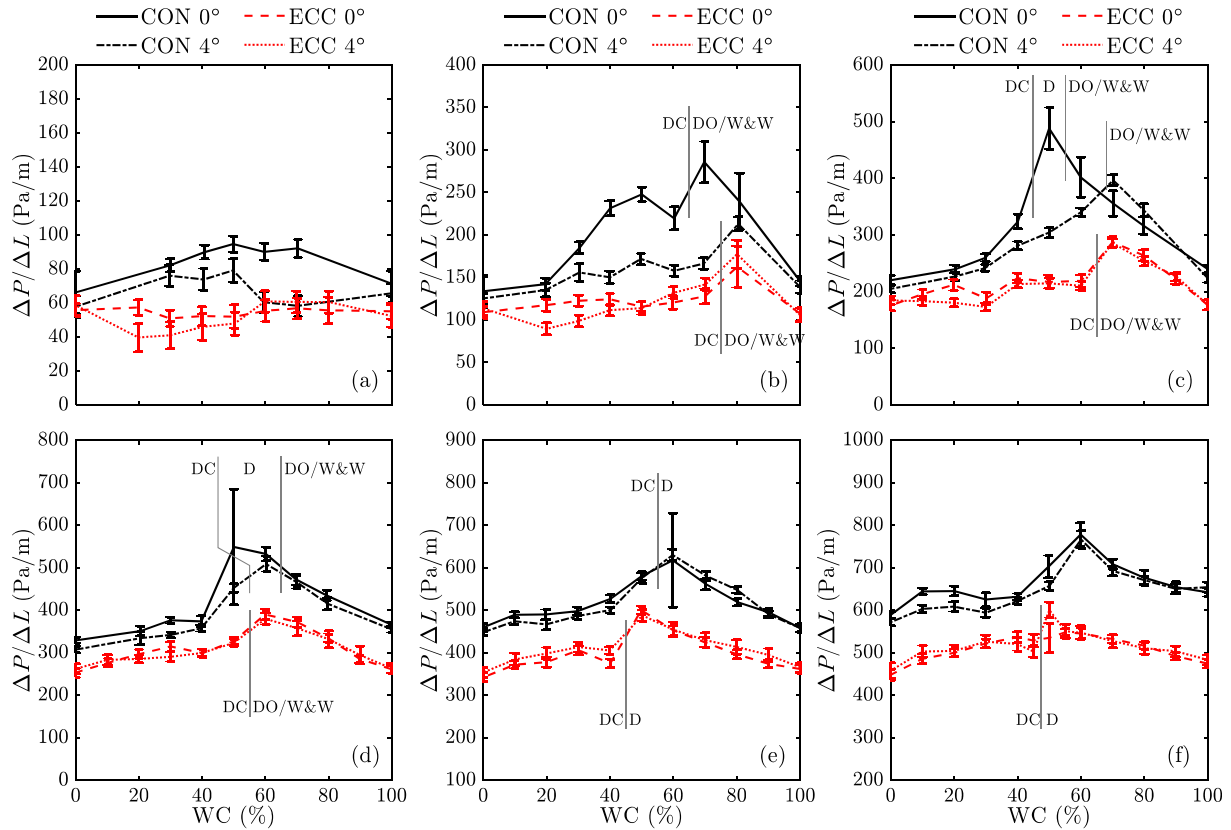
Fig. 11. Frictional pressure gradient, $\Delta P/\Delta L$, as function of the water cut in concentric and fully eccentric annuli at 0° and 4° pipe inclination and mixture velocities, U_M, of: (a) 0.50 m/s, (b) 0.75 m/s, (c) 1.00 m/s, (d) 1.25 m/s, (e) 1.50 m/s, and (f) 1.75 m/s.

Results reveal that the frictional pressure gradient in the concentric annulus, for a given flow condition, is higher than that observed in the fully eccentric annulus. This is in agreement with observations from single-phase and two-phase gas-liquid flows in annuli (see Caetano et al., 1992a; Ibarra et al., 2019). For a given annulus configuration and mixture velocity, similar trends are observed between the two pipe inclinations studied with the exception of low mixture velocities, especially in concentric annulus. At these conditions, the effect of gravity on the flow becomes significant, thus, the velocity of the water phase decreases which in turn increases the water holdup (see Fig. 9).

The occurrence of different flow regimes in the pipe affects the profile of the frictional pressure gradient for a given mixture velocity as the water cut is varied. For stratified flows, the pressure gradient shows a fairly linear profile with the water cut. As droplets are generated, initially flowing at or near the interface (i.e. SWD flow regime), the pressure gradient shows minor variations. Our experimental data reveal two different behaviours as function of the annulus eccentricity (note that SWD is only observed at $U_M = 0.50$ m/s). In the concentric annulus, the two-phase pressure gradient is higher than the single-phase water value at the same mixture velocity. The opposite behaviour is observed in the fully eccentric annulus. The presence of droplets in the flow can generate a drag reduction phenomenon for which the two-phase pressure gradient becomes lower than that obtained in single-phase flow. This phenomenon is attributed to droplet break-up and coalescence for which large droplets can supress turbulence (Pal, 1993; Soleimani, 1999). This behaviour is only observed in the fully eccentric annulus at low mixture velocities (i.e. $U_M \leq 1.00$ m/s), especially at low water cuts. For flows in circular pipes, this phenomenon is more prominent at high mixture velocities for which highly mixed flows are observed (see, for example, Soleimani, 1999; Lovick and Angeli, 2004).

As the mixture velocity increases, dual continuous and dispersed flows are observed. At the transition between these flow regimes (for a constant mixture velocity), a peak in the pressure gradient appears. This can be described as a partial phase inversion phenomenon. Conversely, the pressure gradient peak in the concentric annulus at $U_M = 1.75$ m/s would represent the transition between oil-in-water and water-in-oil dispersion, i.e. full phase inversion. The phase inversion occurs when the dispersed phase becomes the continuous phase and vice-versa. At this point, the effective viscosity of the mixture increases as a result of the droplet structure change (see, for example, experiments in circular pipes by Arirachakaran et al., 1989; Pal, 1993). From our experimental data, as the mixture velocity increases, the peak in the pressure gradient is located at lower water cuts. For example, for fully eccentric annulus, the maximum pressure gradient, for a constant U_M, is observed at WC = 80% for $U_M = 0.75$ m/s, at WC = 60% for $U_M = 1.25$ m/s, and at WC = 50% for $U_M = 1.50$ m/s. A similar trend is observed in the concentric annulus with few variations between 0° and 4° pipe inclination at medium mixture velocities. Kumara et al. (2009) also observed this behaviour in circular pipes using the same test fluids in a steel test section of 56 mm inside diameter, i.e. at $U_M = 0.50$, 1.00 and 1.50 m/s, the peak in the pressure gradient was observed at water cuts of 90%, 81% and 76%, respectively. Note that Kumara et al. (2009) used a similar inlet design than that used in this investigation. Other studies (in circular pipes) have found peaks in the pressure gradient at lower water cuts, e.g. Soleimani (1999) at WC $\approx$ 35% and Elseth (2001) at WC $\approx$ 27%. This difference can be attributed to: (1) lower mixture velocities in our experimental investigation for which fully (homogeneously) dispersed flows are not observed, and (2) the design of the inlet section (i.e. splitter plates) that promotes initially separated flows reducing the level of dispersion along the test section. Note that Elseth (2001) performed experiments using a pre-

homogenised oil-water dispersion which was introduced into the test section using a low shear pump.

3.4.1. Pressure gradient comparison with models

The prediction of pressure gradient in liquid-liquid flow in pipes is commonly performed using either the homogeneous model or the two-fluid model. In the homogeneous model, the two phases are considered to be fully mixed, thus, the mixture can be treated as an effective single-phase flow based on mixture properties. The frictional pressure gradient, in horizontal flow, can be calculated as

$$\frac{\Delta P}{\Delta L} = \frac{2}{D_h} f_M \rho_M U_M^2,$$ (5)

where f_M is the mixture wall friction factor (Fanning) which can be estimated using the modified Caetano et al. (1992a) model for single-phase flow in annuli as presented by Ibarra and Nossen (2018) (see Appendix A). The mixture friction factor is based on the mixture Reynolds number

$$Re_M = \frac{\rho_M U_M^2 D_h}{\mu_M},$$ (6)

where the mixture viscosity, μ_M, can be estimated using several dispersion viscosity models (see Ngan et al., 2009; for a review). In this work, we have used the model of Brinkman (1952)/Roscoe (1952),

$$\frac{\mu_M}{\mu_C} = (1 - \varphi)^{-2.5},$$ (7)

where μ_C is the continuous phase viscosity and φ is the phase fraction of the dispersed phase.

In general, dispersion viscosity models consider complete dispersion having only one continuous phase. However, this is commonly observed mainly at high mixture velocities. As the mixture velocity decreases for a given water cut, the phase fraction of the dispersed phase decreases (lower level of mixing). This means that both phases have continuous layers at a given region of the pipe. Thus, a coefficient has been introduced in the original Brinkman (1952)/Roscoe (1952) model to account for the reduced level of dispersion as

$$\frac{\mu_M}{\mu_C} = (1 - \gamma\varphi)^{-2.5}.$$ (8)

This coefficient is a function of the mixture Froude number, $Fr_M = U_M/\sqrt{gD_h(1 - \rho_O/\rho_W)}$, as follows

$$\begin{cases} \gamma = 1, & Fr_M > Fr_{M\_D}; \\ \gamma = \left(\frac{1-\gamma_{min}}{Fr_{M\_D}-Fr_{M\_SWD}}\right)(Fr_M - Fr_{M\_SWD}) + \gamma_{min}, & Fr_{M\_SWD} \leq Fr_M \leq Fr_{M\_D}; \\ \gamma = \gamma_{min}, & Fr_M < Fr_{M\_SWD}; \end{cases}$$ (9)

where the Froude number at the transition to stratified-wavy with droplets and full dispersion (obtained from the experimental data) are $Fr_{M\_SWD} = 1.62$ and $Fr_{M\_D} = 5.69$, respectively.

The minimum value of the level of dispersion coefficient, γ_{min}, is a function of the annulus eccentricity, and a good approximation to the experimentally observed behaviour is

$$\gamma_{min} = 0.5 - \frac{|E|}{5}.$$ (10)

Note that the coefficient γ_{min} is higher for concentric annulus (i.e. $E = 0$). This is in line with experimental observations which reveal that the level of mixing in the concentric annulus is higher than that observed in the fully eccentric annulus. The selection of the Froude number as the dimensionless parameter to describe the level of dispersion is based on the relevant varying parameters in our experiments (i.e. flow velocity and annulus eccentricity).

Experiments performed using different fluids would be necessary to further expand the applicability of this model, e.g. to include the effect of the interfacial forces on the level of dispersion.

At high water cuts (oil-in-water dispersions), it was observed that the oil phase is completely dispersed in the water phase regardless of the mixture velocity. This corresponds to dispersion of oil-in-water with a water layer (DO/W&W) as presented in Sections 3.1 and 3.2. Thus, the original Brinkman (1952)/Roscoe (1952) model is used for all mixture Froude numbers.

The estimation of the mixture viscosity using the model presented above requires the knowledge of the phase inversion point to determine the continuous and dispersed phase at a given phase fraction. A number of correlations have been developed for the estimation of the inversion point, e.g. Arirachakaran et al. (1989), Nadler and Mewes (1997), and Brauner and Ullmann (2002). In this work, we have adopted the methodology proposed by Ngan et al. (2009) which states that the phase inversion is located at the phase fraction of minimum difference in the mixture viscosities between dispersion of water-in-oil and oil-in-water. The mixture viscosity, for both possible dispersions, is calculated using existing dispersion viscosity models. Fig. 12 shows the estimation of the phase inversion for the test fluids used in this investigation using the modified Brinkman (1952)/Roscoe (1952) model where the coefficient γ is obtained from Eq. (9) for water-in-oil dispersions and $\gamma = 1$ for oil-in-water dispersions.

The predicted phase inversion points (from the graphical method) are located at similar water cuts (with a slight underprediction) compared to where the peaks in the pressure gradient
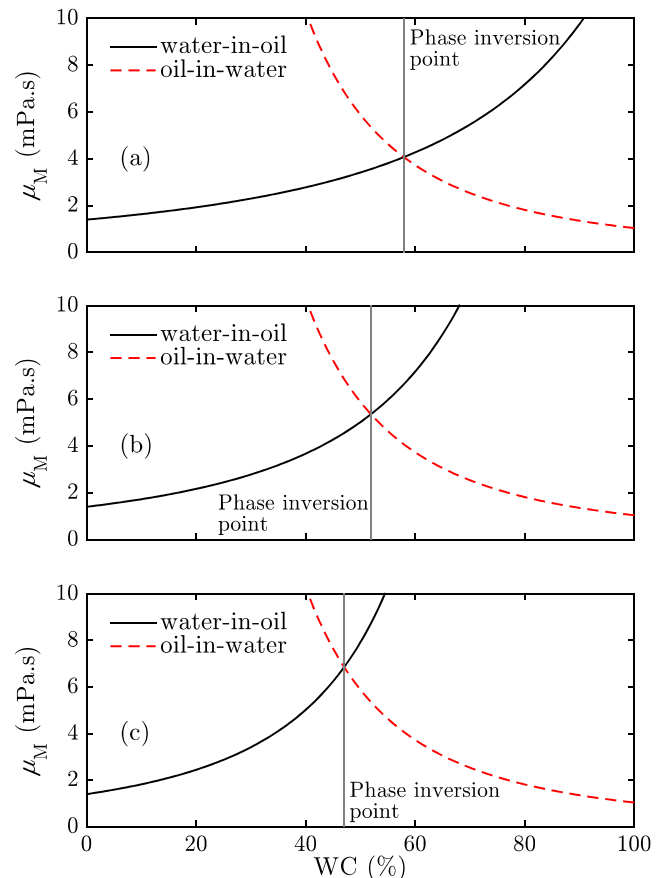

Fig. 12. Prediction of the phase inversion point (PI) using the Ngan et al. (2009) method, for the test fluids used in this work in concentric annulus, based on the modified Brinkman (1952)/Roscoe (1952) viscosity model at mixture velocities, U_M, of: (a) 0.75 m/s (PI = 58%), (b) 1.25 m/s (PI = 52%), and (c) 1.75 m/s (PI = 47%).

were observed in the experiments. For example, in concentric annulus, the maximum pressure gradient, for a constant U_M, in horizontal and 4° upward inclination is observed at WC = 70–80% for U_M = 0.75 m/s, at WC = 50–60% for U_M = 1.25 m/s, and at WC = 60% for U_M = 1.75 m/s. Note that the model predicts phase inversion points at lower water cuts as the mixture velocity increases. This is also observed experimentally.

The second approach considered in this work is the so-called two-fluid model. This is based on the momentum equations of each of the phases in a stratified flow arrangement (Brauner and Moalem Maron, 1989). For fully-developed flow, steady-state, horizontal and co-current flow, the water and oil phase momentum equations are given as follows, respectively,

$$-A_W \frac{\Delta P}{\Delta L} - \tau_W S_W + \tau_i S_i = 0, \tag{11}$$

$$-A_O \frac{\Delta P}{\Delta L} - \tau_O S_O - \tau_i S_i = 0, \tag{12}$$

where A is the cross-sectional area occupied by each phase, S is the contact perimeter, τ is the shear stress and the subscripts 'w', 'o' and 'i' denotes the water phase, the oil phase, and the oil-water interface, respectively. Note that the above equations are written for an oil average velocity higher than the water phase (i.e. $U_O > U_W$).

The combined momentum equation is obtained by equating the pressure term in both phases as

$$\tau_W \frac{S_W}{A_W} - \tau_O \frac{S_O}{A_O} - \tau_i S_i \left(\frac{1}{A_W} + \frac{1}{A_O} \right) = 0. \tag{13}$$

This equation is solved based on the closure relationships presented in Appendix B. Then, the pressure gradient can be calculated from Eqs. (10) or (12).

Fig. 13 and Table 4 show the performance of the pressure gradient predictions using the homogeneous and two-fluid model as compared with the measured experimental data. The modified Brinkman (1952)/Roscoe (1952) viscosity model shows a better performance for data at low mixture velocities in both the concentric and fully eccentric annuli. Conversely, the original Brinkman (1952)/Roscoe (1952) viscosity model estimates higher pressure gradients (i.e. higher mixture viscosity) with a marked peak even at low mixture velocities. The two-fluid model under-predicts the experimental data in both annulus configurations with a drag reduction like-behaviour in the fully eccentric annulus at low water cuts. This is the effect of the inner pipe position on the closure relationships. Note that all three prediction models under-predict the pressure drop for dispersion of oil-in-water with a water layer (DO/W&W). For this flow regime, the highly packed oil-in-water dispersion layer at the top of the pipe seems to have a larger effect on the emulsion viscosity than dual continuous (DC) of fully dispersed flows (D).

The performance of the pressure gradient predictions has also been categorised by flow regime as shown in Tables 5 and 6. Note that the flow regimes have been classified in three main categories: separated flows (SWD), dual continuous (DC and DW&W), and dispersions (D and DO/W&W). This analysis shows that in the fully eccentric annulus, the two-fluid model performs better for separated flows (i.e. SWD) as compared to other flow regimes. Moreover, for SWD, the two-fluid model outperforms the homogenous model using the original Brinkman (1952) viscosity model. However, in concentric annulus, the opposite behaviour is observed, i.e. the two-fluid model shows the highest error against the experimental data for all flow regimes, especially for SWD. This can be attributed to the higher level of mixing observed in the concentric annulus as compared to that in the fully eccentric configuration.
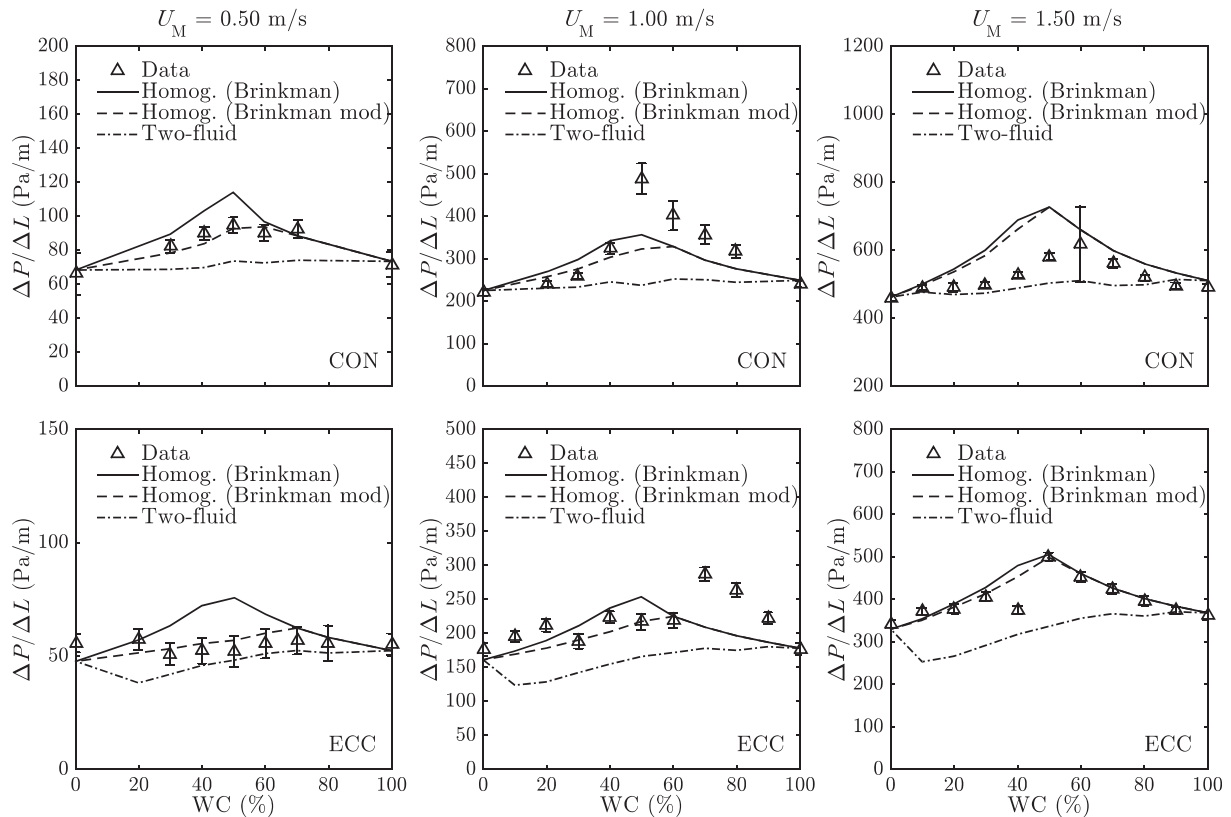

Fig. 13. Frictional pressure gradient, $\Delta P/\Delta L$, comparison with predictions from the homogeneous and two-fluid model in horizontal concentric annulus (top row) and fully eccentric annulus (bottom row) at different mixture velocities.

Table 4
Overall error statistical parameters (see Appendix C for definition) of the frictional pressure gradient models for the horizontal annuli data.

Annulus	Model	e_1 (%)	e_2 (%)	e_3 (%)	R^2
Concentric	Homogeneous (Brinkman, 1952)	5.17	14.82	17.26	0.806
	Homogeneous (modified Brinkman, 1952)	1.32	13.96	17.42	0.811
	Two-fluid model	−16.32	16.83	14.77	0.825
Eccentric	Homogeneous (Brinkman, 1952)	4.80	12.09	15.58	0.924
	Homogeneous (modified Brinkman, 1952)	−0.74	8.97	11.78	0.933
	Two-fluid model	−22.04	22.04	10.54	0.761

Table 5
Error statistical parameters of the frictional pressure gradient models for different flow regimes for the horizontal concentric annulus data.

Regime	Model	e_1 (%)	e_2 (%)	e_3 (%)
SWD	Homogeneous (Brinkman, 1952)	9.49	11.15	9.22
	Homogeneous (modified Brinkman, 1952)	−2.70	4.35	4.18
	Two-fluid model	−20.06	20.06	2.42
DC	Homogeneous (Brinkman, 1952)	9.71	16.00	16.33
	Homogeneous (modified Brinkman, 1952)	2.31	15.52	18.04
	Two-fluid model	−17.56	17.56	14.10
D and DO/W&W	Homogeneous (Brinkman, 1952)	2.35	14.97	18.59
	Homogeneous (modified Brinkman, 1952)	1.62	15.05	18.92
	Two-fluid model	−15.07	15.90	16.45

Thus, the interfacial friction model used in the two-fluid model, for separated flows, would require a modification to account for the partial dispersion near the interfacial region.

4. Conclusions

The co-current flow of oil and water in horizontal and low-inclination upward annuli has been investigated. The annulus flow experiments include a concentric and fully eccentric configuration with a pipe diameter ratio of $K = 0.505$. The experimental data consists of flow regime maps, cross-sectional average water holdup from broad-beam gamma densitometers, and pressure gradient. Flow regime maps were constructed using images from high-speed cameras (shadowgraph) and the analysis of X-ray chordal holdup measurements along the vertical projection.

Five different flow regimes have been identified: (1) stratified-wavy with droplets (SWD), (2) dual continuous (DC), (3) dispersion of oil-in-water with a water layer (DO/W&W), (4) dispersion (D), and (5) dispersion of water-in-oil with a water layer at the bottom (DW/O&W). The latter, which was only observed in the fully eccentric annulus, is characterised by a thin water film that flows at the bottom of the annulus pipe (i.e. in the narrow gap), thus, flowing slower than the dispersed layer above. Experiments reveal that the level of mixing in the concentric annulus is higher than that observed in the fully eccentric annulus. The constructed flow regime maps show that the transition to dispersed flows occurs at lower mixture velocities in the concentric annulus compared to the eccentric annulus. This can be attributed to the effect of the smaller annular gap, as compared to the wider gap at the top region of the eccentric annulus, which affects the velocity distribution promoting instabilities at the interface.

Fully eccentric annulus yields a higher mean water holdup than that in the concentric annulus for a given input water cut and mixture velocity. The higher water accumulation in the fully eccentric annulus can be attributed to the low velocity region in the narrow gap at the annulus pipe bottom. In general, the mean water holdup in both the concentric and fully eccentric annuli is higher than the input water cut (H_W > WC). As the mixture velocity increases, the water holdup approaches the water cut, and thus both phases flow at similar velocities. In the concentric annulus for DO/W&W, the interface between the oil-in-water dispersion layer and the water layer below is wavy, and H_W < WC.

The frictional pressure gradient in the concentric annulus is higher than in fully eccentric annulus for a given inlet condition. Peaks in the pressure gradient, for a constant mixture velocity, are observed at high water cuts (i.e. WC ≥ 50%) at the transition between dispersed (including DO/W&W) and dual continuous flows (partial phase inversion) and between oil-in-water and water-in-oil dispersion (full phase inversion). As the mixture velocity increases, this peak is observed at lower water cuts. The measured pressure gradient data have been compared with predictions using the homogeneous, based on the Brinkman (1952)/

Table 6
Error statistical parameters of the frictional pressure gradient models for different flow regimes for the horizontal fully eccentric annulus data.

Regime	Model	e_1 (%)	e_2 (%)	e_3 (%)
SWD	Homogeneous (Brinkman, 1952)	20.81	20.92	17.24
	Homogeneous (modified Brinkman, 1952)	4.66	7.60	6.95
	Two-fluid model	−13.45	13.45	9.61
DC and DW/O&W	Homogeneous (Brinkman, 1952)	7.31	10.74	11.89
	Homogeneous (modified Brinkman, 1952)	0.36	8.03	10.47
	Two-fluid model	−26.45	26.45	7.23
D and DO/W&W	Homogeneous (Brinkman, 1952)	−3.94	10.68	13.99
	Homogeneous (modified Brinkman, 1952)	−4.01	10.64	13.97
	Two-fluid model	−19.54	19.54	11.99

Roscoe (1952) dispersion viscosity model, and the two-fluid model. In general, the homogeneous model using the modified Brinkman (1952)/Roscoe (1952) viscosity model shows the best agreement with data. This new model provides a more realistic approach by specifying that the level of dispersion is a function of the velocity of the flow, expressed here in nondimensional form as a Froude number. Conversely, the two-fluid model under-predict most of the experimental data. This is expected as this model treats the flow as two separated layers (*i.e.* dispersion effects are not included). Interestingly, the two-fluid model shows reasonable agreement with data for dispersed flows in the concentric annulus at low water cuts (*i.e.* WC < 50%.), especially at U_M = 1.75 m/s. This suggests that, at these flow conditions, the effect of the dispersed phase concentration on the emulsion viscosity is small.

Declaration of Competing Interest

The authors declared that there is no conflict of interest.

Acknowledgements

Appendix A. Single-phase friction factor in annulus

The friction factor in single-phase flows in annuli can be estimated using the Caetano et al. (1992a) model, which was modified and validated by Ibarra and Nossen (2018). This model is based on a geometry parameter, G, that modifies the friction factor in circular pipes, f_{CP}, as follows

$$f_{CON/ECC} = f_{CP}(G_{CON/ECC})^c, \qquad (A.1)$$

where the full pipe Fanning friction factor for laminar flows is estimated as $f_{CP} = 16/Re$. For turbulent flows the Zigrang and Sylvester (1982) correlation can be used

$$\frac{1}{\sqrt{f_{CP}}} = -4\log\left\{\frac{\epsilon}{3.7D_h} - \frac{5.02}{Re}\log\left[\frac{\epsilon}{3.7D_h} - \frac{5.02}{Re}\log\left(\frac{\epsilon}{3.7D_h} + \frac{13}{Re}\right)\right]\right\}, \qquad (A.2)$$

where ϵ is the roughness of the pipe and the Reynolds number is defined as $Re = \rho U D_h / \mu$.

For concentric annulus, the geometry parameter is

$$G_{CON} = K_0 \frac{(1-K)^2}{\frac{1-K^4}{1-K^2} - \frac{1-K^2}{\ln(1/K)}}, \qquad (A.3)$$

where the empirical correction factor K_0 has been introduced to obtain a better performance for a wider range of diameter ratios and is given by

$$K_0 = \max(0.68, K_1), \qquad (A.4)$$

$$K_1 = 1 - |0.56 - K|. \qquad (A.5)$$

For eccentric annulus, the geometry parameter is

$$G_{ECC} = \frac{(1-K)^2(1-K^2)}{4\phi\sinh^4\eta_0}, \qquad (A.6)$$

where

$$\cosh\eta_0 = \frac{K(1-E^2) + (1+E^2)}{2E}, \qquad (A.7)$$

$$\cosh\eta_1 = \frac{K(1+E^2) + (1-E^2)}{2KE}, \qquad (A.8)$$

$$\phi = (\coth\eta_1 - \coth\eta_0)^2\left[\frac{1}{\eta_0 - \eta_1} - 2\sum_{j=1}^{\infty}\frac{2j}{e^{2j\eta_1} - e^{2j\eta_0}}\right]$$
$$+ \frac{1}{4}\left(\frac{1}{\sinh^4\eta_0} - \frac{1}{\sinh^4\eta_1}\right). \qquad (A.9)$$

Finally, the exponent c for laminar flows is equal to unity and for turbulent flows

$$c = 0.45e^{-(Re-3000)/10^6}. \qquad (A.10)$$

Appendix B. Two-fluid model closure relationships

Geometrical considerations

The contact perimeters with the annulus pipe wall and the oil-water interface are written as functions of the inner and outer pipe diameters, the degree of eccentricity, and the height of the water phase, h_W, based on a flat cross-sectional interface in the azimuthal direction. In general, three cases, as shown in Fig. B1, are obtained based on the relative position of the water height with respect to the bottom of the inner pipe, $h^* = (D_1 - D_2)/2 + \delta$, where δ is the distance between the pipe centres.

The water and interfacial perimeter in the annulus configuration are calculated using Table B1 where the perimeters in a circular pipe (S_{W_CP} and S_{i_CP}) are given by

$$S_{W\_CP}(h, D) = D\left[\pi - \cos^{-1}\left(2\frac{h}{D} - 1\right)\right], \qquad (B.1)$$

$$S_{i\_CP}(h, D) = D\sqrt{1 - \left(2\frac{h}{D} - 1\right)^2}, \qquad (B.2)$$

with h and D as the relative bottom layer height and the pipe diameter, respectively, for a generic circular pipe. Finally, the oil interfacial perimeter is calculated as $S_O = \pi(D_1 + D_2) - S_W$.

Shear stress

The shear stress for the water, oil, and interface are defined as

$$\tau_W = \frac{1}{2}f_W\rho_W U_W^2, \qquad (B.3)$$

$$\tau_O = \frac{1}{2}f_O\rho_O U_O^2, \qquad (B.4)$$

$$\tau_i = \frac{1}{2}f_i\rho_j|U_O - U_W|(U_O - U_W), \qquad (B.5)$$
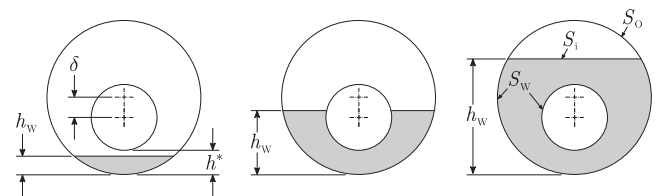
where f is the friction factor.

Fig. B1. Schematic of the two-fluid model geometrical parameters.

Table B1
Calculation of the water and interfacial perimeter in the annulus configuration.

	$h_W \leq h^*$	$h^* < h_W < h^* + D_2$	$h_W \geq h^* + D_2$
Water	$S_W = S_{W\_CP}(h_W, D_1)$	$S_W = S_{W\_CP}(h_W, D_1) + S_{W\_CP}((h_W - h^*), D_2)$	$S_W = S_{W\_CP}(h_W, D_1) + \pi D_2$
Interfacial	$S_i = S_{i\_CP}(h_W, D_1)$	$S_i = S_{i\_CP}(h_W, D_1) - S_{i\_CP}((h_W - h^*), D_2)$	$S_i = S_{i\_CP}(h_W, D_1)$

Friction factor

The water and oil wall friction factor (f_W and f_O) are calculated using the approach presented in Appendix A for flows in annuli with Reynolds numbers defined as

$$Re_W = \frac{\rho_W U_W D_{hW}}{\mu_W}, \tag{B.6}$$

$$Re_O = \frac{\rho_O U_O D_{hO}}{\mu_O}. \tag{B.7}$$

The hydraulic diameters are given as follows

$$D_{hW} = \frac{4A_W}{S_W + S_i}, \quad D_{hO} = \frac{4A_O}{S_O}, \quad \text{for } UW/UO > 1.05 \tag{B.8}$$

$$D_{hW} = \frac{4A_W}{S_W}, \quad D_{hO} = \frac{4A_O}{S_O + S_i}, \quad \text{for } UW/UO < 0.95 \tag{B.9}$$

$$D_{hW} = \frac{4A_W}{S_W}, \quad D_{hO} = \frac{4A_O}{S_O}, \quad \text{for } 0.95 \leq UW/UO \leq 1.05 \tag{B.10}$$

The interfacial friction factor is estimated as

$f_i = m Re_j^{-n}$, (B.11) where coefficients m and n are 16 and 1, respectively, for laminar flow and 0.046 and -0.2 for turbulent flows. The subscript 'j' (for Eqs. (B.5) and (B.11)) is defined from the velocity difference, i.e. j = w for $U_W > U_O$ and j = o for $U_O > U_W$. Finally, the interfacial friction factor, and in turn the interfacial shear stress, are neglected when both phases flow at similar velocities, i.e. $\tau_i = 0$ for $0.95 \leq U_W/U_O \leq 1.05$.

Appendix C. Error statistical parameters

The percentage average relative error, e_1, between the frictional pressure gradient data, $(\Delta P/\Delta L)_{data}$, and predictions, $(\Delta P/\Delta L)_{pred}$, for a total number of samples, N, is

$$e_1(\%) = \left(\frac{1}{N} \sum_i^N \frac{(\Delta P/\Delta L)_{pred,i} - (\Delta P/\Delta L)_{data,i}}{(\Delta P/\Delta L)_{data,i}} \right) \times 100. \tag{C.1}$$

The percentage absolute average relative error, e_2, is

$$e_2(\%) = \left(\frac{1}{N} \sum_i^N \frac{\left| (\Delta P/\Delta L)_{pred,i} - (\Delta P/\Delta L)_{data,i} \right|}{(\Delta P/\Delta L)_{data,i}} \right) \times 100. \tag{C.2}$$

The standard deviation of the relative error, e_3, is

$$e_3(\%) = \sqrt{\frac{1}{N-1} \sum_i^N \left(\frac{(\Delta P/\Delta L)_{pred,i} - (\Delta P/\Delta L)_{data,i}}{(\Delta P/\Delta L)_{data,i}} - \frac{e_1}{100} \right)^2} \times 100. \tag{C.3}$$

The coefficient of determination, R^2, is

$$R^2 = 1 - \frac{\sum_i^N \left((\Delta P/\Delta L)_{data,i} - (\Delta P/\Delta L)_{pred,i} \right)^2}{\sum_i^N \left((\Delta P/\Delta L)_{data,i} - \langle (\Delta P/\Delta L)_{data} \rangle \right)^2}, \tag{C.4}$$

where the mean frictional pressure gradient is $\langle (\Delta P/\Delta L)_{data} \rangle = (\Delta P/\Delta L)_{data}/N$.

References

Angeli, P., Hewitt, G.F., 2000. Flow structure in horizontal oil-water flow. Int. J. Multiph. Flow 26 (7), 139–157.

Arirachakaran, S., Oglesby, K.D., Malinowsky, M.S., Shoham, O., Brill, J.P., 1989. An analysis of oil/water phenomena in horizontal pipes, SPE Paper 18836, SPE Prod. Oper. Symp., Oklahoma City, pp. 155–167.

Brauner, N., Moalem Maron, D., 1989. Two-phase liquid-liquid stratified flow. Physico-Chem. Hydrodynam. 11, 487–506.

Brauner, N., Ullmann, A., 2002. Modeling of phase inversion phenomenon in two-phase pipe flows. Int. J. Multiph. Flow 28, 1177–1204.

Brinkman, H.C., 1952. The viscosity of concentrated suspensions and solutions. J. Chem. Phys. 20 (4), 571.

Caetano, E.F., Shoham, O., Brill, J.P., 1992a. Upward vertical two-phase flow through an annulus-Part I: Single-phase friction factor, Taylor bubble rise velocity, and flow pattern prediction. J. Energy Resour. Technol. 114 (1), 1–13.

Caetano, E.F., Shoham, O., Brill, J.P., 1992b. Upward vertical two-phase flow through an annulus-Part II: Modeling bubble, slug, and annular flow. J. Energy Resour. Technol. 114 (1), 14–30.

Charles, M.E., Govier, G.W., Hodgson, G.W., 1961. The horizontal pipeline flow of equal density oil-water mixtures. Can. J. Chem. Eng. 39 (1), 27–36.

Conan, C., Masbernat, O., Decarre, S., Line, A., 2007. Local hydrodynamics in a dispersed-stratified liquid-liquid pipe flow. AIChE 53 (11), 2754–2768.

Dieck, R.H., 2006. Measurement Uncertainty: Methods and Applications, Fourth ed. ISA.

Elseth, G. 2001. An experimental study of oil/water flow in horizontal pipes. Ph.D. Thesis, NTNU.

Harvel, G.D., Hori, K., Kawanishi, K., Chang, J.S., 1999. Cross-sectional void fraction distribution measurments in a vertical annulus two-phase flow by high speed X-ray computed tomography and real-time neutron radiography techniques. Flow Meas. Instrum. 10, 259–266.

Hasan, A.R., Kabir, C.S., 1992. Two-phase flow in vertical and inclined annuli. Int. J. Multiph. Flow 18 (2), 279–293.

Hibiki, T., Situ, R., Mi, Y., Ishii, M., 2003. Local flow measurements of vertical upward bubbly flow in an annulus. Int. J. Heat Mass Tran. 46 (1479–1496).

Hu, B., Langsholt, M., Liu, L., Andersson, P., Lawrence, C., 2014. Flow structure and phase distribution in stratified and slug flows measured by X-ray tomography. Int. J. Multiph. Flow 67, 162–179.

Ibarra, R., Markides, C.N., Matar, O.K., 2014. A review of liquid-liquid flow patterns in horizontal and slightly inclined pipes. Multiphase Sci. Technol. 26 (3), 171–198.

Ibarra, R., Nossen, J., 2018. Bubble velocity in horizontal and low-inclination upward slug flow in concentric and fully eccentric annuli. Chem. Eng. Sci. 192, 774–787.

Ibarra, R., Zadrazil, I., Matar, O.K., Markides, C.N., 2018. Dynamics of liquid–liquid flows in horizontal pipes using simultaneous two–line planar laser–induced fluorescence and particle velocimetry. Int. J. Multiph. Flow 101, 47–63.

Ibarra, R., Nossen, J., Tutkun, M., 2019. Two-phase gas-liquid flow in concentric and fully eccentric annuli. Part I: Flow patterns, holdup, slip ratio and pressure gradient. Chem. Eng. Sci. 203, 489–500.

Izwan Ismail, A.S., Ismail, I., Zoveidavianpoor, M., Mohsin, R., Piroozian, A., Misnan, M.S., Sariman, M.Z., 2015. Review of oil-water through pipes. Flow Meas. Instrum. 45, 357–374.

Julia, J.E., Ozar, B., Jeong, J.-J., Hibiki, T., Ishii, M., 2011. Flow regime development analysis in adiabatic upward two-phase flow in a vertical annulus. Int. J. Heat Fluid Flow 32, 164–175.

Kelessidis, V.C., Dukler, A.E., 1989. Modeling flow pattern transitions for upward gas-liquid flow in vertical concentric and eccentric annuli. Int. J. Multiph. Flow 15 (2), 173–191.

Kumara, W.A.S., Halvorsen, B.M., Melaaen, M.C., 2009. Pressure drop, flow pattern and local water volume fraction measurements of oil-water flow in pipes. Meas. Sci. Technol. 20, (11) 114004.

Kumara, W.A.S., Halvorsen, B.M., Melaaen, M.C., 2010. Particle image velocimetry for characterizing the flow structure of oil-water flow in horizontal and slightly inclined pipes. Chem. Eng. Sci. 65, 4332–4349.

Liu, L., Matar, O.K., Lawrence, C.J., Hewitt, G.F., 2006. Laser-induced fluorescence (LIF) studies of liquid–liquid flows. Part I: Flow structures and phase inversion. Chem. Eng. Sci. 61 (12), 4007–4021.

Lovick, J., Angeli, P., 2004. Experimental studies on the dual continuous flow pattern in oil-water flows. Int. J. Multiph. Flow 30, 139–157.

Lum, J.Y.L., Al-Wahaibi, T., Angeli, P., 2006. Upward and downward inclination oil-water flows. Int. J. Multiph. Flow 32, 413–435.

Morgan, R.G., Markides, C.N., Zadrazil, I., Hewitt, G.F., 2013. Characteristics of horizontal liquid–liquid flows in a circular pipe using simultaneous high-speed laser-induced fluorescence and particle velocimetry. Int. J. Multiph. Flow 49, 99–118.

Morgan, R.G., Ibarra, R., Zadrazil, I., Matar, O.K., Hewitt, G.F., Markides, C.N., 2017. On the role of buoyancy-driven instabilities in horizontal liquid–liquid flow. Int. J. Multiph. Flow 89, 123–135.

Moyers-Gonzalez, M.A., Frigaard, I.A., 2007. Kinematic instabilities in two-layer eccentric annular flows, part 1: Newtonian fluids. J. Eng. Math. 62, 103–131.

Nadler, M., Mewes, D., 1997. Flow induced emulsification in the flow of two immiscible liquids in horizontal pipes. Int. J. Multiph. Flow 23 (1), 55–68.

Ngan, K.H., Ioannou, K., Rhyne, L.D., Wang, W., Angeli, P., 2009. A methodology for predicting phase inversion during liquid-liquid dispersed pipeline flow. Chem. Eng. Res. Des. 87, 318–324.

Pal, R., 1993. Pipeline flow of unstable and surfactant-stabilised emulsions. AIChE J. 39, 1754–1764.

Pouplin, A., Masbernat, O., Decarre, S., Line, A., 2011. Wall friction and effective viscosity of a homogeneous dispersed liquid-liquid flow in a horizontal pipe. AIChE 57 (5), 1119–1131.

Prieto, L., Muñoz, F., Pereyra, E., Ratkovich, N., 2018. Pressure gradient correlations analysis for liquid-liquid flow in horizontal pipes. J. Pet. Sci. and Eng. 169, 683–704.

Roscoe, R., 1952. The viscosity of suspensions of rigid spheres. Br. J. Appl. Phys. 3, 267–269.

Russell, T.W.F., Hodgson, G.W., Govier, G.W., 1959. Horizontal pipeline flow of mixtures of oil and water. Can. J. Chem. Eng. 37 (1), 9–17.

Shahidi, M.K., Ozbelge, T.A., 1995. Direct contact heat transfer between two immiscible liquids flowing in a horizontal concentric annulus. Int. J. Multiph. Flow 21 (6), 1025–1036.

Soleimani, A. 1999. Phase distribution and associated phenomena in oil-water flows in horizontal tubes. Ph.D., Imperial College London.

Torres, C.F., Mohan, R.S., Gomez, L.E., Shoham, O., 2016. Oil-water flow pattern transition prediction in horizontal pipes. J. Energy Resour. Technol. 138, (2) 022904.

Trallero, J.L. 1995. Oil-Water Flow Pattern in Horizontal Pipes. Ph.D. Thesis, The University of Tulsa.

Zigrang, D.J., Sylvester, N.D., 1982. Explicit approximations to the solution of Colebrook's friction factor equation. AIChE 28 (3), 514–515.